https://doi.org/10.1016/j.scitotenv.2018.12.209

Is Himalayan-Tibetan Plateau “Drying”? Historical estimations and future trends of surface soil moisture

Qiang Zhang, Keke Fan, Vijay P. Singh, Changqing Song, Chong-Yu Xu, Peng Sun

Corresponding author:

Qiang Zhang, Ph.D. Professor,

Key Laboratory of Environmental Changes and Natural Hazards, Ministry of Education (Director), & Academy of Disaster Reduction and Emergency Management, Ministry of Civil Affairs, Ministry of Education (Dean)

Beijing Normal University,

Beijing 100875,

China.

Tel: +86-10-58807086

E-mail: zhangq68@bnu.edu.cn (preferred contact address)

Mr. Keke Fan

Key Laboratory of Environmental Changes and Natural Hazards, Ministry of Education; Academy of Disaster Reduction and Emergency Management, Ministry of Civil Affairs, Ministry of Education

Beijing Normal University,

Beijing 100875,

E-mail: fankk@mail.bnu.edu.cn (preferred contact address)

https://doi.org/10.1016/j.scitotenv.2018.12.209

Is Himalayan-Tibetan Plateau "Drying"? Historical estimations and future trends of surface soil moisture

Qiang Zhang[1,2,3*], Keke Fan[1,2,3*], Vijay P. Singh[4], Changqing Song[1,2,3], Chong-Yu Xu[5], Peng Sun[6]

1. Key Laboratory of Environmental Change and Natural Disaster, Ministry of Education, Beijing Normal University, Beijing 100875, China;
2. Faculty of Geographical Science, Academy of Disaster Reduction and Emergency Management, Ministry of Education/Ministry of Civil Affairs, Beijing Normal University, Beijing 100875, China;
3. State Key Laboratory of Earth Surface Processes and Resources Ecology, Beijing Normal University, Beijing 100875, China;
4. Department of Biological and Agricultural Engineering and Zachry Department of Civil Engineering, Texas A&M University, College Station, Texas, USA;
5. Department of Geosciences, Oslo University, Blindern 0316, Oslo, Norway;
6. College of Territorial Resource and Tourism, Anhui Normal University, Anhui 241002, China;

Abstract The Himalayan-Tibetan Plateau (HTP), often known as the "Third Pole" and the "Asian Water Tower", is the source of water resources for many Asian rivers and in turn for hundreds of millions of people living downstream. The HTP has direct impacts on the establishment and maintenance of Asian monsoon, and therefore on the climate of its surrounding areas. Besides, soil moisture plays a critical role in the hydrological cycle and is a critical link between land surface and atmosphere. Hence, soil moisture was greatly emphasized by Global Climate Observing System Programme as an Essential Climate Variable. However, little is known about soil moisture changes on the HTP from a long-term perspective. By comparing remotely sensed and modelled soil moisture datasets against in-situ observations from 100 observation stations, here we find that Noah performed better than other soil moisture datasets. In past years, soil moisture first decreased and then increased obviously. In most regions on HTP, precipitation changes can be taken as the major cause behind soil moisture variations. In future, there is persistently decreasing soil moisture trend since ~2010 with a decreasing rate of -0.044 kg/m^2/10a, -0.031 kg/m^2/10a and -0.0p 88 kg/m^2/10a under RCP2.6, RCP4.5 and RCP8.5 scenarios, respectively, in CMIP5 (Coupled Model Intercomparision Project Phase 5). Specifically, a sudden decrease of soil moisture with a rate of -0.372 kg/m^2/10a can be expected after ~2080 under RCP8.5 scenario. Amplifying terrestrial aridity due to increasing precipitation but more significant increasing potential evapotranspiration potentially results in drying HTP. Potential water deficiency for Asian rivers due to drying HTP should arouse considerable concerns.

Key words: Soil moisture; Historical observations; CMIP5 data; Himalayan-Tibetan Plateau

1. Introduction

Soil moisture is a pivotal link between the land surface and atmosphere mainly through hydrothermal exchange (Albergel et al., 2013; Wanders et al., 2014; Zeng et al., 2015), and plays a critical role in the hydrological cycle (Wanders et al., 2014), shifting of vegetation species (Rous et al., 2013), and change in microbial activity, and modification of warming-induced soil C losses (Crowther et al., 2016). Soil moisture is also a state variable controlling the land surface energy partition, surface runoff, soil drainage, and soil-freeze-thaw status (Seneviratne et al., 2010; Yang et al., 2013; Zhang et al., 2015), as well as for numerical weather prediction and climate projections (Albergel et al., 2013). Therefore, soil moisture was taken seriously by the Global Climate Observing System (GCOS) Programme that recognized it as an Essential Climate Variable (ECV) (Albergel et al., 2013).

The HTP, known as the Third Pole and "the roof of the world," has an average elevation of over 4000 m above sea level (Yang et al., 2013; Zhang et al., 2013; Bai et al., 2016). The HTP is also known as the "Asian Water Tower", because it is the source of many major Asian rivers, such as Brahmaputra (Yaluzangbu), Salween (Nu), Mekong (Lancang), Yellow, and Yangtze rivers (Zhang et al., 2013; Immerzeel et al., 2009), and these rivers supply water for hundreds of millions of people living downstream (Zhang et al., 2013). Therefore, it is important to understand soil moisture changes from a long-term perspective on the HTP, which is most sensitive to global changes, and enhance our knowledge of the land-atmosphere interactions and potential impacts on the climate of East and Southeast Asia (Hsu and Liu, 2003; Zeng et al., 2015) exhibited by shifting soil thermal regime and soil thermal conductivity (Subin et al., 2013). However, little is known about the future trend of soil moisture on the HTP and related main drivers, with the exception of some investigations on soil moisture changes derived from remotely sensed dataset and observation network (Su et al., 2011; Yang et al., 2013; Zeng et al., 2015).

Due to the importance of soil moisture changes and also the role that soil moisture changes have in shifting impacts of HTP on surrounding climate, there are many researches addressing evaluations of reanalysis and remote sensing soil moisture data on HTP. Based on soil moisture and temperature datasets collected from a monitoring network consisting of 55 stations in the central HTP, Chen et al. (2013) evaluated four soil moisture products retrieved from the Advanced Microwave Scanning Radiometer-Earth Observing System (AMSR-E) and four land surface modelling products from the Global Land Data Assimilation System (GLDAS) using the station-averaged surface SM (soil moisture) data from the network and found that these four GLDAS models tended to systematically underestimate the surface SM. Comparison was done by Su et al. (2011) for three remote sensing retrievals, i.e. AMSR-E, ASCAT-L2, and SMOS, against the soil moisture datasets from the Tibet-Obs network (the Tibetan Plateau observation of plateau scale soil moisture and soil temperature) and results indicated that different soil moisture datasets had markedly different performances in different climate regions. Besides, Su et al. (2013), based on two regional SM and soil temperature networks (i.e., Naqu and Maqu) on the HTP, conducted SM analysis using the European Centre for Medium-Range Weather Forecasts (ECMWF) previous optimum interpolation scheme and the current point-wise extended Kalman filter scheme, and concluded that this method improved accuracy of the estimated SM. Zeng et al. (2015) analyzed in-situ SM measurements from three networks which represented different climatic and vegetation conditions over the HTP with aim to evaluate seven remotel sensed SM products (AMSR-E, AMSR2, SMOS, ECV) and one reanalysis SM product (ERA-Interim) during 2002-2012 and pointed out that in general ECV and ERA-Interim outperformed the other datasets. Bi et al. (2016) evaluated the SM simulated from four land surface models (LSM) (Mosaic, Noah, Community Land Model, and Variable Infiltration Capacity) in GLDAS-1 and the more recent GLDAS-2 against in-situ SM measurements collected from two SM networks located on the HTP at different soil depths and found that Noah estimated the soil moisture with less bias.

It should be underlined that above-mentioned researches have done some evaluations on different remotely sensed and/or reanalysis assimilation soil moisture data against in-situ soil moisture measurements from one, two and/or even three soil moisture networks on the HTP (e.g. Dente et al., 2012). And owing to different in-situ soil moisture datasets utilized to evaluate reanalysis and/or remotely sensed soil moisture data, different evaluation results can be expected. Besides, variations of soil moisture in both space and time and related causes were not quantified. Meanwhile, another important scientific issue is that what tendencies of soil moisture are in the future under different climatic scenarios. Scientific answer of this issue is of great theoretical and scientific significance in terms of variability and availability evaluations of soil moisture mass under different climatic scenarios. Therefore, shifts of hydrothermal properties of HTP due to different soil moisture changes under different climatic scenarios and related impacts of HTP on its surrounding climate can be well understood. Therefore, the objectives of this study are: (1) to evaluate reanalysis and remotely sensed soil moisture data against in-situ soil moisture observations based on all available soil moisture data from three soil moisture observation networks; (2) to quantify different causes behind SM variations with respect to precipitation, temperature, and so on; and (3) to quantify changing tendencies of soil moisture during decades to come. This study can help to bridge the knowledge gap between soil moisture data evaluation of last decades and changing tendencies during decades to come under different climatic scenarios.

2. Data

2.1 Observed SM

These two sets of measured SM datasets, Tibet-Obs, and CTP-SMTMN (a multiscale SM and Temperature Monitoring Network on the central Tibet Plateau) were utilized in this study as “true” SM to verify the estimated SM (Table S1). (1) Tibet-Obs covers 43 measuring stations in three regional scale in-situ reference networks (Fig. 1; Table 1), including 18 sites in the cold arid Ngari network, 5 sites in the cold semiarid Naqu network and 20 sites in the cold humid Maqu network in total. The measuring probes were installed at different depths for different soil layers in these three networks. And in Ngari and Maqu networks, the probes were placed at the depth of 5 cm for the upper soil moisture which means they can measure 0-10 cm SM, however, 0-5 cm for the upper layer of SM in the Naqu network. These networks provide a representative coverage of the different climate and land surface hydrometeorological conditions on the HTP (Su et al., 2011). (2) CTP-SMTMN lies around Naqu in a cold semiarid climate with an average elevation of over 4500m above mean sea level (a.m.s.l), and it comprises 57 measuring sites. At each site, one probe was installed obliquely into 0-5 cm topsoil, but other three were inserted horizontally at the depths of 10 cm, 20 cm, and 40 cm depths (Chen et al., 2013; Yang et al., 2013). As for the Naqu network, the depth of the SM measurement is consistent for other two different datasets.

2.2 Reanalysis and remotely sensed soil moisture data

The ECV soil moisture product is the first purely multi-decadal satellite-based soil moisture product covering a period of November 1978 to December 2013. It is a daily data with a spatial resolution of 0.25° which was developed as part of Water Cycle Multimission Observation Strategy (WACMOS) and Soil Moisture Climate Change Initiative (CCI) projects by the European Space Agency (ESA) (Liu et al., 2011; Liu et al., 2012; Gruber et al., 2017). The ECV soil moisture product was merged by the passive remotely sensed datasets covering the Scanning Multichannel Microwave Radiometer onboard Nimbus-7, the Special Sensor Microwave Imager of the Defense Meteorological Satellite Program, the Tropical Rainfall Measuring Mission Microwave Imager, the AMSR-E onboard the Aqua satellite, the WindSat satellite, and the AMSR2 boarded on the GCOM-W1 satellite, and the active datasets covering the scatterometers onboard the European Remote Sensing satellites and the ASCAT onboard the MetOp-A satellite. This set of SM just comprises C-band satellite SM data which, in general, represents SM content of the top shallow 0-2 cm surface soil layer.

ERA-Interim is the latest global atmospheric reanalysis product produced by the European Centre for Medium Range Weather Forecasts (ECMWF) covering the period from1 January 1979 to present, continuously updated in real time (Dee et al., 2011). A fixed version of NWP (numerical weather prediction) system, which assured that no spurious trends were introduced, was utilized to produce this data. Meanwhile, this system merged or assimilated observations with a foregoing forecast to obtain the best fit. SM is available every 6 hours (0, 6, 12, 18 UTC) with four soil layers (0-7, 7-28, 28-100, 100-289 cm) (Zeng et al., 2015). The ERA-Interim daily averaged SM on the upper layer with a 0.25°×0.25° scale was employed for the evaluation. MERRA (the Modern-Era Retrospective analysis for Research and Application, Version 2) is a re-analysis dataset that combines in-situ and remotely sensed observations of atmospheric conditions, radiance data from sounders, and wind retrievals from scatterometers beginning from 1980 which replaces the original MERRA dataset owing to the processes in the assimilation system with an updated version of GEOS (the Goddard Earth Observing System) model (Rienecker et al., 2011). MERRA is the first global reanalysis dataset with long-term space-based observations of aerosols and interactions with other physical processes in the land-atmosphere system. The MERRA-L dataset is a land-only analysis with meteorological forcing from MERRA model and more realistic precipitation forcing. Here, the hourly upper layer (0-2 cm) SM data was employed which was produced on a 0.625°×0.5° resolution and then resampled to 0.25°×0.25° so as to keep all datasets consistent by the inverse distance weight interpolation technique.

The Global Land Data Assimilation System (GLDAS) is developed to produce optimal evaluations of land surface states and fluxes by integrating satellite- and station-based observational data products and data assimilation techniques into land surface models (Rodell et al., 2004). GLDAS data can be available at the website of GES DISC (the Goddard Earth Sciences Data and Information Services Center, http://disc.sci.gsfc.nasa.gov/hydrology/data-holdings). In this current study, two Noah datasets were used owing to different time intervals of these two datasets, that is, V2.0 (1948-2010), and V2.1 (2000-2017). The time interval the observed soil moisture covering is during 2008-2013. Therefore, Noah V2.0 and Noah V2.1 were both used. To verify this feasibility of this analysis, cross verification was done and Noah V2.0 dataset was used to analyze historical changes of soil moisture.

2.3. Climate variables

The China Meteorological Forcing Dataset is a set of near-surface meteorological and environmental reanalysis data sets developed by the Institute of Tibetan Plateau, Chinese Academy of Sciences (Table S2). This dataset covers the period of 1979-2010 and were produced by merging multisource datasets, including Princeton forcing data, GLDAS data, GEWEX-SRB radiation data, TRMM satellite precipitation data and China Meteorological Administration (CMA). This dataset of version 1.0 currently was completed and publicly available with a temporal resolution of 3 hours and a horizontal spatial resolution of 0.1°×0.1°, consisting of a total of seven variables, that is, air temperature, pressure, air specific humidity, wind, surface downward shortwave radiation (SDSR), surface downward longwave radiation, precipitation (Yang et al., 2010).

2.4. Climatological model data in CMIP5

At a worldwide meeting in September 2008, the WCRP's Working Group on

Coupled Modeling (WGCM) invited 20 climate simulation organizations around the world and promoted a new set of coordinated climate experiments. These experiments consisted of the fifth phase of the Coupled Model Intercomparison Project (CMIP5). CMIP5 will provide a multi-model context for: 1) exploring the mechanisms of model differences in poorly understood feedbacks with the carbon cycle and clouds; 2) studying climate predictability on decadal time scales; and 3) investigating why similarly forced models lead to notably different responses. The CMIP is a standard framework for studying the output of coupled land-atmosphere-ocean general circulation models (GCM). In this study, we used 26 GCMs output of CMIP5 with surface SM and 41 models with climate variables, such as, precipitation and temperature, which are listed in detail in Tables S3 and S4, respectively. And 41 GCMs with precipitation, max temperature, min temperature, relative humidity and wind speed were employed to explore the potential causes behind SM variations (Table S4). The outputs of all GCMs used can be obtained from https://esgf-node.llnl.gov/projects/esgf-llnl/.

3. Analysis procedure and methods

3.1 Assessment method of estimated soil moisture data

We collected the available in-situ soil moisture observations (Su et al., 2011; Chen et al., 2013) and subdivided these data points into 0.25°×0.25º grids (27 grids in total: 5 in Ngari; 12 in Naqu; 10 in Maqu). The mean soil moisture value of each grid was obtained by averaging all data points falling within that grid pixel (Chen et al., 2013). The same analysis was done on remotely sensed and reanalysis SM datasets and climate variables which had been interpolated into 0.25°×0.25° in order to keep all the cells consistent (Chen et al., 2013; Zeng et al., 2015). Analysis of correlation between observed and remotely sensed and assimilated soil moisture data indicated that Noah_2.1 better described observed soil moisture changes than ECV, ERA and MERRA during 2008-2014. The correlation analysis was performed by Pearson correlation analysis technique, Spearman correlation analysis technique and Kendall correlation analysis method, and different calculation methods similarly led to the consistent result. Therefore, Fig. 2 just illustrates the nonparametric Spearman correlation coefficient and the advantage of which is that it is not necessary to assume the normal distribution of the data and the results are not affected by monotonous changes. We also evaluated the performance of Noah_2.0 and Noah_2.1 in describing observed soil moisture changes due to the different time spans, that is, Noah_2.0 in 1948-2010 and Noah_2.1 in 2000-present, respectively (Chen et al., 2013). In the evaluation periods of 2008-2014, Noah_2.1 is superior to the others in general and the analysis during the period of overlap for Noah_2.0 and Noah_2.1, 2008-2010, found that Noah_2.0 slightly better modelled observed soil moisture than Noah_2.1 did. Hence, Noah_2.0 was used to analyze historical soil moisture changes.

3.2 Method for diagnosing the causes behind SM changes

To determine major causes of soil moisture changes, we used a stepwise multivariate regression method to differentiate principle drivers behind soil moisture changes, and AIC (the Akaike's information criterion) index was chosen as the criterion to accept or reject the variables. Then we utilized multiple GLM (the general linear model) regressions to quantify the fractional contribution of each meteorological variable in the CMA data set to Noah soil moisture changes (Tao et al., 2015). Then, we obtained 11 GCM models out of the 26 available CMIP5 GCMs (General Circulation Models, Table S4) with SM variable which have a correlation coefficient over 0 with Noah SM and further investigation was done on the future SM changes based on these 11 GCM models under three scenarios, i.e. RCP2.6， RCP4.5， RCP8.5 (upper panel of Fig. 5; Table S4) with confidence intervals (Fu and Feng, 2014). In addition, the causes of future soil changes were also analyzed, based on analysis of precipitation, terrestrial evapotranspiration, and aridity index (P/PET, P refers to precipitation and PET refers to potential evapotranspiration) based on 41 CMIP5 GCMs (Fu and Feng, 2014).

4. Results and discussions

4.1 Performance of ECV, ERA, MERRA and Noah soil moisture datasets

Three regional scale in-situ reference networks for plateau scale soil moisture were considered (Fig. 1) and these networks provided a representative coverage of different climate and land surface hydrometeorological conditions on the HTP (Su et al., 2011). Fig. 2 shows grid-scale correlation between ECV, ERA, MERRA and Noah soil moisture datasets and in-situ soil moisture observations. It can be seen from Fig. 2 that all reanalysis and remotely sensed moisture data seem to well describe in-situ soil moisture observations with large correlation coefficients. However, in general, correlation coefficients between Noah soil moisture data and in-situ soil moisture observations are larger than those between ECV, ERA, MERRA and in-situ soil moisture observations, implying that Noah data can better describe in-situ soil moisture changes. Fig. S1 shows temporal changes of ECV, ERA, MERRA and in-situ soil moisture observations with confidence interval of the in-situ observed soil moisture data by ARIMA method. It can be observed that ECV, ERA, MERRA and Noah SMs have different performance in describing changing properties of soil moisture in different observation networks. However, Noah SM data has relative stable performance benchmarked with in-situ observations.

Table S2 indicates there is a time divergence for Noah_2.0 with 1948-2010, and Noah_2.1 with 2000 onwards. Due to time limit, Noah_2.1 is not appropriate for the attribution analysis in spite of the comparison with other data sets. So reliability of Noah_2.0 need exploring further. Fig. 3 show that the comparison between monthly soil moisture for Noah_2.0 and Noah_2.1 during the overlapping period (2008-2010). The results indicate, in 27 grids of 0.25°×0.25º, R^2 of these two data sets of SM more than 0.9 lies in most grids and the data points are almost evenly distributed near the fitted line. In total, the MAE value is about 1.7, comparatively, RMSE value is approximately equal to 2.3. Meanwhile, the histograms indicate R^2 is mainly concentrated in high value area, however, MAE and RMSE are in low value area. The line graph in bottom panel additionally shows Noah_2.0 performs better than Noah_2.1 with in situ soil moisture even with relatively small amounts of data. All results indicate Noah_2.0 can be taken as substitute to conduct attribution analysis.

4.2 Historical SM trends

Additional work with focus on the possible drivers of modeled and observed trends was remarkably underlined (Albergel et al., 2013). Fig. 4 shows identification of major factors influencing soil moisture changes based on stepwise regressive technique and multiple general linear model (GLM) regression. The numbers marked by different colors denote the fractional contribution of each potential driver to soil moisture changes (Fig. 4). It can be seen from Fig. 4 that precipitation has larger fractional contribution to soil moisture changes in majority of regions across the HTP with fractional contribution of > 60% and even > 80%. However, for temperature, wind speed and solar radiation, only smaller part of regions are dominated by fractional contribution of > 80% and most parts of the regions have fractional contributions of less than 40%. Therefore, it can be concluded that precipitation is the most important driver of soil moisture changes compared to the other three studied on the HTP, although fractional contribution of precipitation to soil moisture changes shows notable spatial variability. Fig. 5 illustrates historical observations and future trends of soil moisture changes. It can be observed from upper panel of Fig. 5 that time interval during 1950-2010 is characterized by evident fluctuations of soil moisture amount. Decreasing soil moisture can be detected during ~1950-1970. Subsequent time interval, i.e. 1970-2010, is dominated by persistently increasing soil moisture though moderate changes and decreasing tendency of soil moisture can be found during respectively ~1975-1995 and 2005-2010.

4.3 Future trends of soil moisture

Importance of detection of future trends in soil moisture was emphasized (Albergel et al., 2013). Different changing tendencies of soil moisture under different climatic scenarios were quantified based on outputs of 26 GCM models from CMIP5 with modelling results of the surface soil moisture under scenarios of RCP2.6, RCP4.5 and RCP8.5 (Table S4). Fig. 5 (upper panel) indicates persistently decreasing soil moisture after 2010 with different decreasing rates during different time intervals, such as -0.044kg/m^2/10a, -0.031kg/m^2/10a, -0.088kg/m^2/10a under RCP2.6, RCP4.5 and RCP8.5 scenarios. Meanwhile, decreasing rate of soil moisture under RCP8.5 is two times larger than that under RCP2.6. Sudden decrease of soil moisture can be identified during ~2085-~2100 and it is particularly true for soil moisture under RCP8.5 with decreasing rate of -0.372kg/m^2/10a. Therefore, higher warming intensity is related to larger decreasing rate of soil moisture. There are some researches addressing future trends of soil moisture at different spatial scales. Cheng et al. (2015), based on the output from 20 models of CMIP5 following the RCP4.5 and RCP8.5, indicated a clear decreasing trend occurred over a period of 63 years with pronounced drying over northeast China, north China, part of Mongolia, and Russia near lake Baikal. As for drivers behind soil moisture changes, Cheng et al. (2015) indicated that soil drying is caused mainly by decreasing precipitation but enhanced almost twofold by warming climate. However, different spatial patterns of precipitation regimes can be expected (Li et al., 2013). Therefore, potential drivers behind soil moisture changes should be subject to further and thorough analysis.

4.4 Causes behind soil moisture changes

Precipitation was the major driver of decreased soil moisture. Whether the decreasing soil moisture should be attributed to decreasing or increasing precipitation should be carefully investigated and clarified (Cheng et al., 2015). In our study, the fractional contribution of precipitation to soil moisture was ~≤50% which is derived from the average of the contribution in Fig. 4. Meanwhile, temperature was another important factor which may impact SM through melting permafrost and snow/glacial. While, the increasing rate of evapotranspiration larger than that of precipitation was reported at the global scale, i.e. the rate of increase in precipitation averaged over land was ~1.7%/°C, while the increase in PET was 5.3%/°C, leading to a decrease in P/PET, or a drier terrestrial climate, by ~3.4%/°C (Fu and Feng, 2014). Similarly, increasing precipitation can be expected on the HTP (Fig. 6). However, the increasing rate of evapotranspiration larger than that of precipitation was detected (Fig. 7). The increasing amounts were, respectively, 2.2~3.1%, 1.2~1.4%, 4.9~8.7% for precipitation and were 1.4~2.3%, 3.8~7.1%, 11.9~16.3% for evapotranspiration under RCP2.6, RCP4.5 and RCP8.5, respectively, among different GCMs in CMIP5 in the whole 21st century. It can be observed that the increasing rate of evapotranspiration was 2~3 times larger than that of precipitation, causing drier soil moisture on the HTP (lower panel of Fig. 5). Fu and Feng (2014) also observed increases in precipitation and potential evapotranspiration but a decrease in P/PET due to increasing CO_2 concentration in the

https://doi.org/10.1016/j.scitotenv.2018.12.209

atmosphere in the CMIP5 transient CO_2 1%/year increase experiments. Here, we can attribute decreasing soil moisture to decreased P/PET in the decades to come.

4.5 Coupling of SM anomaly, precipitation, and evapotranspiration

Under future scenarios, soil moisture continues decreasing even with evident fluctuations (Fig. 5). Fig. 6 and Fig. 7 also indicate that there are increasing trend for different radiative scenarios, especially RCP8.5. So it is necessary to further explore the relationship among these three variables. Fig. 8 shows the relationship of precipitation, evapotranspiration and soil moisture anomaly in the future under three scenarios. Evapotranspiration is increasing along with the more energy and more available water due to increasing temperature and precipitation respectively, so there is a positive relationship between evapotranspiration and precipitation (Fig. 8).

With increasing radiation, precipitation per unit leads to more evapotranspiration, the coefficients are respectively 0.10, 0.37, and 0.52 under RCP2.6, RCP4.5 and RCP8.5, which indicates half precipitation is gone via evapotranspiration, and the other half transforms into surface flow, underwater, and other forms of water (Table 2). The relation is evident for both variables under RCP4.5, RCP 8.5, but with P-value of 0.102 under RCP2.6 (Fig. 8). Precipitation is not evidently different for RCP2.6 and RCP4.5, but RCP8.5 results in more precipitation. Soil moisture anomaly is 6.5 10-^{3}kg/m^{2}, more than baseline period due to the high soil moisture in immediate future, which is probably relative with increasing melting ice and snow. The aridity index is 1.61, minimal value among three scenarios, which, in theory, lead to low soil moisture, further verifying the abundant effect of melting ice and snow in subsequent years. Under RCP2.6 scenario, soil moisture anomaly is not evidently related with precipitation and evapotranspiration without visual regularity (Fig. 8). Under RCP4.5 and RCP8.5, the more the precipitation, the more the evapotranspiration, and the less the soil moisture anomaly. The phenomenon is most remarkable under RCP8.5 with higher variability of soil moisture anomaly which is consistent with the results from Figs. 5-7.

5. Discussions

In this study, we utilized the in-situ SM as the benchmark to choose the best fitted estimated SM datasets including ECV, ERA, MERRA and Noah. Then Noah_2.0 was used to explore SM changes and the fractional contribution of each individual meteorological variable to SM was evaluated. Finally, the outputs of CMIP models were employed to analyze future SM changes and to explore potential causes behind SM changes. Obviously, much uncertainty could be expected in the historical estimation of the SM datasets which may reach unreliable conclusions. The uncertainty can be attributed mainly to the following causes: different depths of the uppermost soil layer; different spatial scales, inaccuracy of different data acquisition methods including measuring instrument, remote sensing retrieval algorithm, model parameterization and so on, which have been discussed in the research by Zhang et al. (2018). In these procedures, there exists a lot of tough problems, and the most serious one of which is the discrepancy of upper layer SM from different SM sources. It is well known that the

ECV SM data is produced from satellite remote sensing technology which generally represents SM changes of the upper shallow 1-2 cm soil layer. ERA-Interim SM dataset contains four layers of soil moisture data (0-7cm, 7-28cm, 28-100cm, 100-289cm). In this study, we evaluated the SM in the surface soil layer of 0-7cm. The SM by the MERRA is used in the top soil layer of 0-2cm. Noah model in GLDAS has four layers of soil moisture data, i.e. 0-10, 10-40, 40-100, and 100-200cm. The SM of the uppermost soil layer (0-10) was used in this study. What's more, the upper soil layer depth of GCM models is 10 cm for the future SM analysis. Although there are mismatching in different SM datasets, the range of the soil thickness is small, and so we assume that the change of soil moisture in the quite thin upper soil layer is not obvious. Meanwhile, previous studies have indicated that the SM is one of the hydrological variables difficult to be measured accurately. The SM measurement is affected by a range of factors, such as man-made operation, instrument sensitivity, and probe depth and so on. So the measured SM values are varying from different measurement processes. And the GCM models also have a relatively poor performance for modelling of SM. Therefore, to reduce these uncertainties, we used the z-score method to normalize the SM for all SM datasets.

The Tibetan Plateau is known as "the third pole" with extremely complex topographies and climates, thus leading to different vegetation covers over the entire region (Fan et al., 2018). In particular, large parts of the HTP are covered by permafrost and snow/ice due to the high elevation. So the performance of these estimated SM remains largely varying from one specific region to another. The soil hydraulic properties can have great impacts on the simulation of the upper soil moisture. Meanwhile, the simulated evaporation can also influence the modelling of the soil moisture. Each of them is quite difficult to be expressed accurately in the model (Chen et al., 2013). In addition, due to complex topography, the in situ observation stations were installed mainly in the relatively flat area without harsh ambient environment. Although the distribution of the stations is as even as possible and different spatial scales are used to evaluate the data (Chen et al., 2013; Zhang et al., 2018) which greatly corroborated the representativeness of the measured data. The variables in the CMIP have predicted the future climate which is the hot spot in the research on climate change. In accordance with practice, here we used the median value as the prediction of the upper soil moisture in the future. In order to reduce the uncertainty, we collected as many data sets as possible containing surface soil moisture. Otherwise, it is indispensable to up-scale soil moisture resolution in consideration of better evaluation results on a larger scale and high spatial variability of soil moisture, the soil moisture output of GCMs are resampled uniformly to the spatial scale of 1°×1°.

The soil moisture and its variability have a strong control on the generation of runoff and characterize the regional response to precipitation changes (Penna et al., 2011), and hence directly influence the size of water bodies. In this case, historical observations of soil moisture changes can be further evidenced by researches pertaining lake sizes, snow and glacial melting processes and water mass of the HTP as well. Analyses of lake sizes during the 1960s-1980s and 2005-2006 indicated increases in lake sizes in the Tibet Plateau and its neighboring provinces with an appearance of 60 new lakes (Ma et al., 2010). Meanwhile, glaciers on the Tibetan Plateau have been melting at an accelerating rate over the past decade (Yao et al., 2004; Xu et al., 2009; Ma et al., 2010), leading to increasing water resources (Ma et al., 2010; Yao et al., 2004; Kehrwald et al., 2008) and consequently resulting in increased soil moisture in recent decades (upper panel of Fig. 5). Specifically, a severe shrinkage of lakes during 1970-1990 and a remarkable expansion of a majority of lakes during 1990-2011 were identified on the HTP with an increased total lake area from 35638.11 km^2 in the early 1970s to 41938.66 km^2 in 2011 (Song et al., 2013). These changes of lake areas matched soil moisture changes during similar time intervals. Increased SM during the past few decades was supposed to account for part of the increased mass balance by GRACE which, however, was not explained by the glacier mass gain and the mass increase of lakes (Zhang et al., 2013). Otherwise, the increasing precipitation is also likely to be an important cause behind SM increase during this period (Wan et al., 2017).

6. Summary and conclusions

In this study, the performances of several remotely sensed and reanalysis SM datasets were benchmarked with SM observations from 100 sites at the HTP. In addition, future trends of soil moisture were quantified based on outputs from 26 models of CMIP. Some interesting and important conclusions and findings were achieved as follows:

(1) Noah_2.1 outperformed the other datasets, such as ECV, ERA and MERRA, in the evaluation period of 2008-2014. Noah_2.0 slightly better depicted the SM than Noah_2.1 in the overlapping period.

(2) Different time intervals can be identified with different changing properties of soil

moisture. Decreasing soil moisture can be detected during ~1950-1970. Subsequent time interval, i.e. 1970-2010, is dominated by persistently increasing soil moisture though moderate changes and decreasing tendency of soil moisture can be found during respectively ~1975-1995 and 2005-2010. Soil moisture changes during different time intervals are in line with shifts in lake sizes, melting processes of snow and glacial and also water mass balance on the HTP.

(3) Precipitation was the major driver of decreased soil moisture. However, the fractional contribution of precipitation to soil moisture was ~≤50%. And temperature is also an important cause behind spatiotemporal changes of soil moisture by leading to melting snow and increased evapotranspiration due to warming climate on the HTP. In addition, increasing rate of evapotranspiration is larger than that of precipitation and then leads to increased aridity, i.e. P/PET. Significant increase of aridity due to warming climate may be the major driver behind decreased soil moisture and this point is in line with results at global scale.

Acknowledgments We would like to thank the National Natural Science Foundation of China. This project was largely funded by grants to Qiang Zhang from National Science Foundation for Distinguished Young Scholars of China (Grant No.: 51425903). Peng Sun was supported by Natural Science Foundation of China (Grant No.: 41601023). In addition, the in-situ soil moisture observations are available at http://ismn.geo.tuwien.ac.at/; GLDAS data are available at http://disc.sci.gsfc.nasa.gov/hydrology/data-holdings; ECV soil moisture data are

https://doi.org/10.1016/j.scitotenv.2018.12.209

available at http://www.esa-soilmoisture-cci.org/. The last but not the least, our cordial gratitude should be extended to the editor, Dr. Ralf Ludwig, for his pertinent and professional comments and suggestions which are greatly helpful for further quality improvement of this current manuscript.

References

Albergel, C., Dorigo, W., Reichle, R.H., Balsamo, G., De Rosnay, P., Munoz-Sabater, J., Isaksen, L., De Jeu, R., Wagner, W., 2013. Skill and global trend analysis of soil moisture from reanalysis and microwave remote sensing. J. Hydrometeorol. 14 (4), 1259-1277.

Bai, P., Liu, X., Yang, T., Liang, K., Liu, C., 2016. Evaluation of streamflow simulation results of land surface models in GLDAS on the Tibetan plateau. J. Geophys. Res.-Atmos. 121 (20), 12180-12197.

Bi, H., Ma, J., Zheng, W., Zeng, J., 2016. Comparison of soil moisture in GLDAS model simulations and in situ observations over the Tibetan Plateau. J. Geophys. Res.-Atmos. 121(6), 2658-2678.

Chen, Y., Yang, K., Qin, J., Zhao, L., Tang, W., Han, M., 2013. Evaluation of AMSR-E retrievals and GLDAS simulations against observations of a soil moisture network on the central Tibetan Plateau. J. Geophys. Res.-Atmos. 118(10), 4466-4475.

Cheng, S., Guan, X., Huang, J., Ji, F., Guo, R., 2015. Long-term trend and variability of soil moisture over East Asia. J. Geophys. Res.-Atmos. 120 (17), 8658-8670.

https://doi.org/10.1016/j.scitotenv.2018.12.209

Crowther, T.W. K.E.O. Todd-Brown, C.W. Rowe, W.R. Wieder, J.C. Carey, M.B. Machmuller, B. L. Snoek, S. Fang, G. Zhou, S. D. Allison, J. M. Blair, S.D. Bridgham, A. J. Burton, Y. Carrillo, P. B. Reich, J. S. Clark, A. T. Classen, F. A. Dijkstra, B. Elberling, B. A. Emmett, M. Estiarte, S. D. Frey, J. Guo, J. Harte, L. Jiang, B. R. Johnson, G. Kröel-Dulay, K. S. Larsen, H. Laudon, J. M. Lavallee, Y. Luo, M. Lupascu, L. N. Ma, S. Marhan, A. Michelsen, J. Mohan, S. Niu, E. Pendall, J. Peñuelas, L. Pfeifer-Meister, C. Poll, S. Reinsch, L. L. Reynolds, I. K. Schmidt, S. Sistla, N. W. Sokol, P. H. Templer, K. K. Treseder, J. M. Welker, M. A. Bradford, 2016. Quantifying global soil carbon losses in response to warming. Nature 540 (7631), 104-110.

Dee, D. P., Uppala, S.M., Simmons, A.J., Berrisford, P., Poli, P., Kobayashi, S., Bechtold, P., 2011. The ERA‐Interim reanalysis: Configuration and performance of the data assimilation system. Q. J. R. Meteorol. Soc. 137 (656), 553-597.

Dente, L., Vekerdy, Z., Wen, J., Su, Z., 2012. Maqu network for validation of satellite-derived soil moisture products. Int. J. Appl. Earth Obs. Geoinf. 17, 55-65.

Fan, K., Zhang, Q., Singh, V. P., Sun, P., Song, C., Zhu, X., Yu, H., Shen, Z., 2019. Spatiotemporal impact of soil moisture on air temperature across the Tibet Plateau. Sci. Total Environ. 649, 1338-1348.

Fu, Q., Feng, S., 2014. Responses of terrestrial aridity to global warming. J. Geophys. Res.-Atmos. 119 (13), 7863-7875.

Gruber, A., Dorigo, W.A., Crow, W., Wagner, W., 2017. Triple collocation-based merging of satellite soil moisture retrievals. IEEE Trans. Geosci. Remote. 55(12), 6780-6792.

Hsu, H.H., Liu, X., 2003. Relationship between the Tibetan Plateau heating and East Asian summer monsoon rainfall. Geophys. Res. Lett. 30 (20), 2066. https://doi.org/10.1029/2003GL017909.

Immerzeel, W.W., Droogers, P., De Jong, S.M., Bierkens, M.F.P., 2009. Large-scale monitoring of snow cover and runoff simulation in Himalayan river basins using remote sensing. Remote Sens. Environ. 113(1), 40-49.

Kehrwald, N.M., Thompson, L.G., Yao, T., Mosley‐Thompson, E., Schotterer, U., Alfimov, V., Beer, J., Eikenberg, J., Davis, M.E, 2008. Mass loss on Himalayan glacier endangers water resources. Geophys. Res. Lett. 35 (22), L22503. https://doi.org/10.1029/2008 GL035556.

Li, J., Zhang, Q., Chen, Y.D., Xu, C.Y., Singh, V.P., 2013. Changing spatiotemporal patterns of precipitation extremes in China during 2071-2100 based on Earth System Models. J. Geophys. Res.-Atmos., 118 (22), 12537-12555.

Liu, Y. Y., Parinussa, R.M., Dorigo, W.A., De Jeu, R.A., Wagner, W., Van Dijk, A.I.J.M., McCabe, M.F., Evans, J.P., 2011. Developing an improved soil moisture dataset by blending passive and active microwave satellite-based retrievals. Hydrol. Earth Syst. Sci. 15 (2), 425-436.

Liu, Y.Y., Dorigo, W.A., Parinussa, R.M., De Jeu, R.A., Wagner, W., McCabe, M.F., Evans, J.P., Van Dijk, A.I.J.M., 2012. Trend-preserving blending of passive and active microwave soil moisture retrievals. Remote Sens. Environ. 123, 280-297.

Ma, R., Duan, H., Hu, C., Feng, X., Li, A., Ju, W., Jiang, J., Yang, G., 2010. A half-century of changes in China's lakes: global warming or human influences. Geophys. Res. Lett. 37 (24), L24106. https://doi.org/10.1029/2010GL045514.

Penna, D., Tromp-van Meerveld, H.J., Gobbi, A., Borga, M., Dalla Fontana, G., 2011. The influence of soil moisture on threshold runoff generation processes in an alpine headwater catchment. Hydrol. Earth Syst. Sci. 15 (3), 689-702.

Rienecker, M.M., Suarez, M.J., Gelaro, R., Todling, R., Bacmeister, J., Liu, E., M.G. Bosilovich, S.D. Schubert, L. Takacs, G.-K. Kim, S. Bloom, J. Chen, D. Collins, A. Conaty, A. da Silva, W.Gu, J. Joiner, R.D. Koster, R. Lucchesi, A. Molod, T. Owens, S. Pawson, P. Pegion, C.R. Redder, R. Reichle, F.R. Robertson, A;G. Ruddick, M. Sienkiewicz, J. Woollen, 2011. MERRA: NASA's modern-era retrospective analysis for research and applications. J. Clim. 24(14), 3624-3648.

Rodell, M., Houser, P.R., Jambor, U.E.A., Gottschalck, J., Mitchell, K., Meng, C.J., K. Arsenault, B. Cosgrove, J. Radakovich, M. Bosilovich, J.K. Entin, J.P. Walker, D. Lohmann & D. Toll, 2004. The global land data assimilation system. Bull. Amer. Meteorol. Soc. 85(3), 381-394.

Rous, C.P., Aalto, J., Luoto, M., 2013. Soil moisture's underestimated role in climate change impact modelling in low-energy systems. Glob. Change Biol. 19 (10), 2965-2975.

Seneviratne, S.I., Corti, T., Davin, E.L., Hirschi, M., Jaeger, B.E., Lehner, I., Orlowsky, B., Teuling, J.A., 2010. Investigating soil moisture–climate interactions in a changing climate: A review. Earth Sci. Rev. 99(3-4), 125-161.

Song, C., Huang, B., Ke, L., 2013. Modeling and analysis of lake water storage changes on the Tibetan Plateau using multi-mission satellite data. Remote Sens. Environ. 135, 25-35.

Su, Z., Wen, J., Dente, L., Velde, R., Wang, L., Ma, Y., Yang, K., Hu, Z., 2011. The Tibetan Plateau observatory of plateau scale soil moisture and soil temperature (Tibet-Obs) for quantifying uncertainties in coarse resolution satellite and model products. Hydrol. Earth Syst. Sci. 15 (7), 2303-2316.

Su, Z., Rosnay, P., Wen, J., Wang, L., Zeng, Y., 2013. Evaluation of ECMWF's soil moisture analyses using observations on the Tibetan Plateau. J. Geophys. Res.-Atmos. 118(11), 5304-5318.

Subin, Z.M., Koven, C.D., Riley, W.J., Torn, M.S., Lawrence, D.M., Swenson, S.C., 2013. Effects of soil moisture on the responses of soil temperatures to climate change in cold regions. J. Clim. 26 (10), 3139-3158.

Tao, S., Fang, J., Zhao, X., Zhao, S., Shen, H., Hu, H., Tang, Z., Wang, Z., Guo, Q., 2015. Rapid loss of lakes on the Mongolian Plateau. Proc. Natl. Acad. Sci. 112 (7), 2281-2286.

Wan, G., Yang, M., Liu, Z., Wang, X., Liang, X., 2017. The precipitation variations in the Qinghai-Xizang (Tibetan) Plateau during 1961–2015. Atmosphere 8(5), 80. https://doi.org/10.3390/atmos8050080.

Wanders, N., Bierkens, M.F.P., Jong, S.M., Roo, A., Karssenberg, D., 2014. The benefits of using remotely sensed soil moisture in parameter identification of large-scale hydrological models. Water Resour. Res. 50 (8), 6874-6891.

Xu, B., Cao, J., Hansen, J., Yao, T., Joswia, D.R., Wang, N., Wu, G., Wang, M., Zhao, H., Yang, W., Liu, X., He, J., 2009. Black soot and the survival of Tibetan glaciers. Proc. Natl. Acad. Sci. 106 (22), 22114-22118.

Yang, K., He, J., Tang, W., Qin, J., Cheng, C.C., 2010. On downward shortwave and longwave radiations over high altitude regions: Observation and modeling in the Tibetan Plateau. Agric. For. Meteorol. 150 (1), 38-46.

Yang, K., Qin, J., Zhao, L., Chen, Y., Tang, W., Han, M., Lazhu, Chen, Z., Lv, N., Ding, B., Wu, H., Lin, C., 2013. A multiscale soil moisture and freeze-thaw monitoring network on the third pole. Bull. Amer. Meteor. Soc. 94 (12), 1907-1916.

Yao, T., Wang, Y., Liu, S., Pu, J., Shen, Y., Lu, A., 2004. Recent glacier retreat in High Asia in China and its impact on water resource in northwest China. Sci. China-Earth Sci. 47 (12), 1065-1075.

Zeng, J., Li, Z., Chen, Q., Bi, H., Qiu, J., Zou, P., 2015. Evaluation of remotely sensed and reanalysis soil moisture products over the Tibetan Plateau using in-situ observations. Remote Sens. Environ. 163, 91-110.

Zhang, G., Yao, T., Xie, H., Kang, S., Lei, Y., 2013. Increased mass over the Tibetan Plateau: From lakes or glaciers? Geophys. Res. Lett. 40 (10), 2125-2130.

Zhang, L., Su, F., Yang, D., Hao, Z. Tong, K., 2013. Discharge regime and simulation for the upstream of major rivers over Tibetan Plateau. J. Geophys. Res.-Atmos. 118 (15), 8500-8518.

Zhang, Q., Xiao, M., Singh, V.P., Liu, L., Xu, C.Y., 2015. Observational evidence of summer precipitation deficit-temperature coupling in China. J. Geophys. Res.-Atmos. 120(19), 10040-10049.

Zhang, Q., Fan, K., Singh, V. P., Sun, P., Shi, P., 2018. Evaluation of remotely sensed and reanalysis soil moisture against in situ observations on the Himalayan-Tibetan plateau. J. Geophys. Res.-Atmos. 123 (14), 7132-7148.

Figure captions:

Fig. 1. Locations of Himalayan-Tibetan Plateau (HTP) and spatial distribution of the in-situ stations in three soil moisture networks, i.e. Ngari, Naqu and Maqu. The red closed line refers to the border of HTP. These in-situ networks provide a representative coverage of the different climate and land surface hydrometeorological conditions on the HTP. Ngari is characterized by a cold-arid environment, Naqu by a cold-semiarid environment and Maqu by a cold-humid environment. Filled circles denote locations of the in-situ observation stations for soil moisture, wherein, orange marked sites from Tibet-Obs networks, blue marked ones from ISMN networks.

Fig. 2. Nonparametric Spearman correlation coefficients between in-situ observed soil moisture and remotely sensed and reanalysis soil moisture products on the Himalayan-Tibetan Plateau (HTP). The reanalysis soil moisture data are respectively from European Space Agency's (ESA) Soil Moisture Essential Climate Variable (ECV) CCI project, the second Modern-Era Retrospective analysis for Research and Applications (MERRA-2), European Centre for Medium-Range Weather Forecasts (ECMWF) and NASA Goddard Earth Sciences Data and Information Services

https://doi.org/10.1016/j.scitotenv.2018.12.209

Center (GES DISC). The correlation coefficients indicate that reanalysis soil moisture dataset, the monthly 0.25° GLDAS Version 2 products (GLDAS-2) by Noah model (Noah_2.1), can well quantify soil moisture changes on the HTP.

Fig. 3. Correlations between monthly Noah_2.0 soil moisture data and Noah_2.1 soil moisture data during 2008-2010 from the perspective of R2, MAE (mean absolute error) and RMSE (root mean square error) for the period of 2000-2010 at 27 observation grids (the first panel). The histograms show the distribution of R2, MAE and RMSE. In the bottom panel, the left axis shows changes of R2 between Noah_2.0 soil moisture data (blue curve) and Noah_2.1 soil moisture data (red curve) with in-situ observed soil moisture data in different grids (Fig. 1); the right axis shows the number of months with time overlap, which is represented as a black line.

Fig. 4. Identification of major drivers for soil moisture changes (Noah_2.0) during 1979-2010 using stepwise regressive technique and multiple general linear model (GLM) regression. The stepwise regressive technique was used to screen out the principle drivers behind soil moisture changes, and the multiple general linear model (GLM) regression was used to quantify fractional contributions of each principle driver to soil moisture changes. The analysis was done on each pixel. The numbers marked by different colors denote the fractional contribution of each potential driver to soil moisture changes. Based on the spatial pattern of fractional contributions, precipitation acts as the major driver behind soil moisture changes across most regions of the HTP.

Fig. 5. Soil moisture anomaly during 1948-2010 and 2010-2100 based on remotely

sensed and reanalysis soil moisture data in the whole Himalayan-Tibetan Plateau by 26 models under three scenarios: RCP2.6, RCP4.5 and RCP8.5. In the upper panel, the β values show changing rates of soil moisture during different time intervals (unit: $kg/m^2/10a$) by the Sen's slope method. The shaded areas denote the 95% confidence interval by Student-*t* distribution. The lower panel shows future changes of the aridity index based on remotely sensed and reanalysis dataset by 22 models under RCP2.6, RCP4.5 and RCP8.5 scenarios.

Fig. 6. Future changes of precipitation based on remotely sensed and reanalysis dataset by 40 models under RCP2.5, RCP4.6 and RCP8.5 scenarios (27 models for RCP2.6, 37 models for RCP4.5 and 40 models for RCP8.5).

Fig. 7. Future changes of Penman-Monteith evapotranspiration based on remotely sensed and reanalysis dataset by 23 models under RCP2.6, RCP4.5 and RCP8.5 scenarios (15 models for RCP2.6, 23 models for RCP4.5 and 20 models for RCP8.5).

Fig. 8. Relationships between precipitation, evapotranspiration, and soil moisture anomaly in the future (2010-2100) under RCP2.6 (a), RCP4.5 (b) and RCP8.5 (c). Scatter points denote median values of precipitation, evapotranspiration, and soil moisture anomaly. The gray dashed lines indicate the mean values of precipitation (vertical) and evapotranspiration (horizontal). The blue lines shows fitted results by linear model with 95% confident interval.

Table captions:

Table 1. 26 GCM models from CMIP5 with modelling results of the surface soil

moisture under scenarios of RCP2.6, RCP4.5 and RCP8.5. The detailed information of model can be found in supplementary files.

Table 2. The statistical mean value for precipitation (Pr), evapotranspiration (ET), soil moisture anomaly (SMA) and aridity index (AI) in the future under three scenarios, that is, RCP2.6, RCP4.5 and RCP8.5. Slope is the coefficient of evapotranspiration with precipitation. P-value indicates whether or not there exists evident relationship.

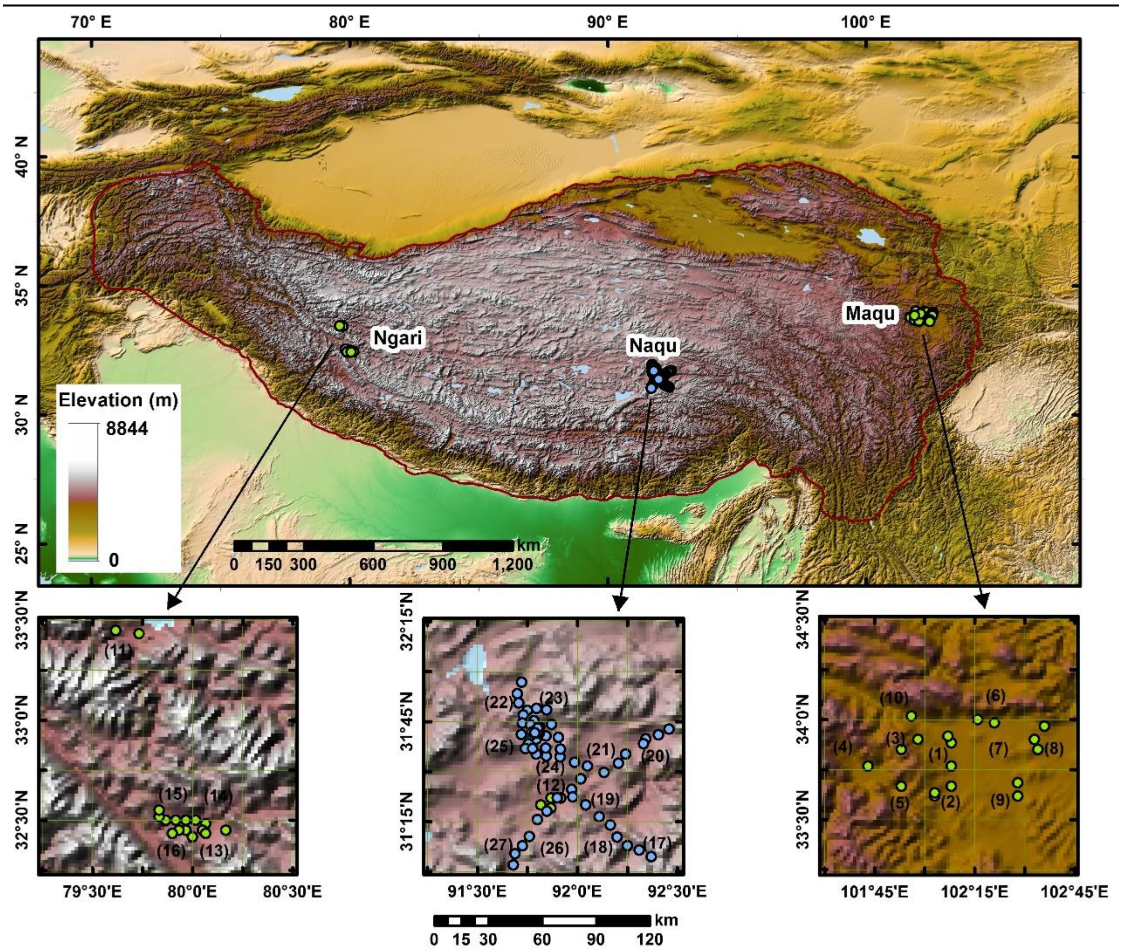

Fig. 1. Locations of Himalayan-Tibetan Plateau (HTP) and spatial distribution of the in-situ stations in three soil moisture networks, i.e. Ngari, Naqu and Maqu. The red line refers to the border of the HTP. These in situ soil moisture observatory networks provide a representative coverage of the different climate and land surface hydrometeorological conditions on the HTP. Ngari is characterized by a cold-arid environment, Naqu by a cold-semiarid environment and Maqu by a cold-humid environment. Filled circles denote locations of the in-situ observation stations for soil moisture, wherein, orange marked sites from Tibet-Obs networks, blue marked ones from ISMN networks.

https://doi.org/10.1016/j.scitotenv.2018.12.209

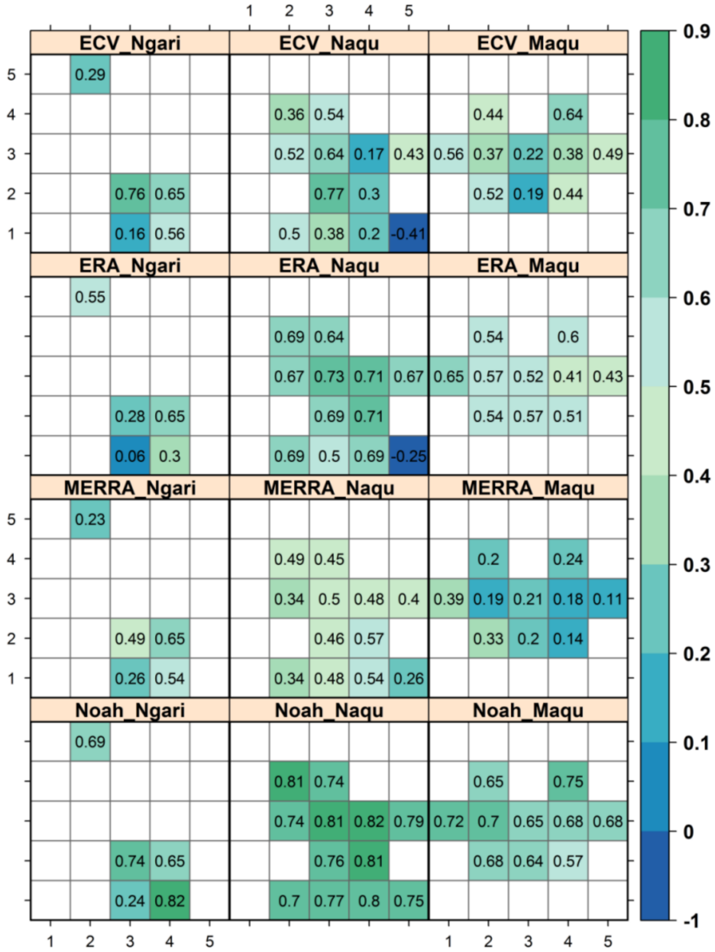

Fig. 2. Nonparametric Spearman correlation coefficients between in-situ observed soil moisture and remotely sensed and reanalysis soil moisture products on the Himalayan-Tibetan Plateau (HTP). The reanalysis soil moisture data are respectively from European Space Agency's (ESA) Soil Moisture Essential Climate Variable (ECV) CCI project, the second Modern-Era Retrospective analysis for Research and Applications (MERRA-2), European Centre for Medium-Range Weather Forecasts (ECMWF) and NASA Goddard Earth Sciences Data and Information Services Center (GES DISC). The correlation coefficients indicate that reanalysis soil moisture dataset, the monthly 0.25° GLDAS Version 2 products (GLDAS-2) by Noah model (Noah_2.1), can well quantify soil moisture changes on the HTP.

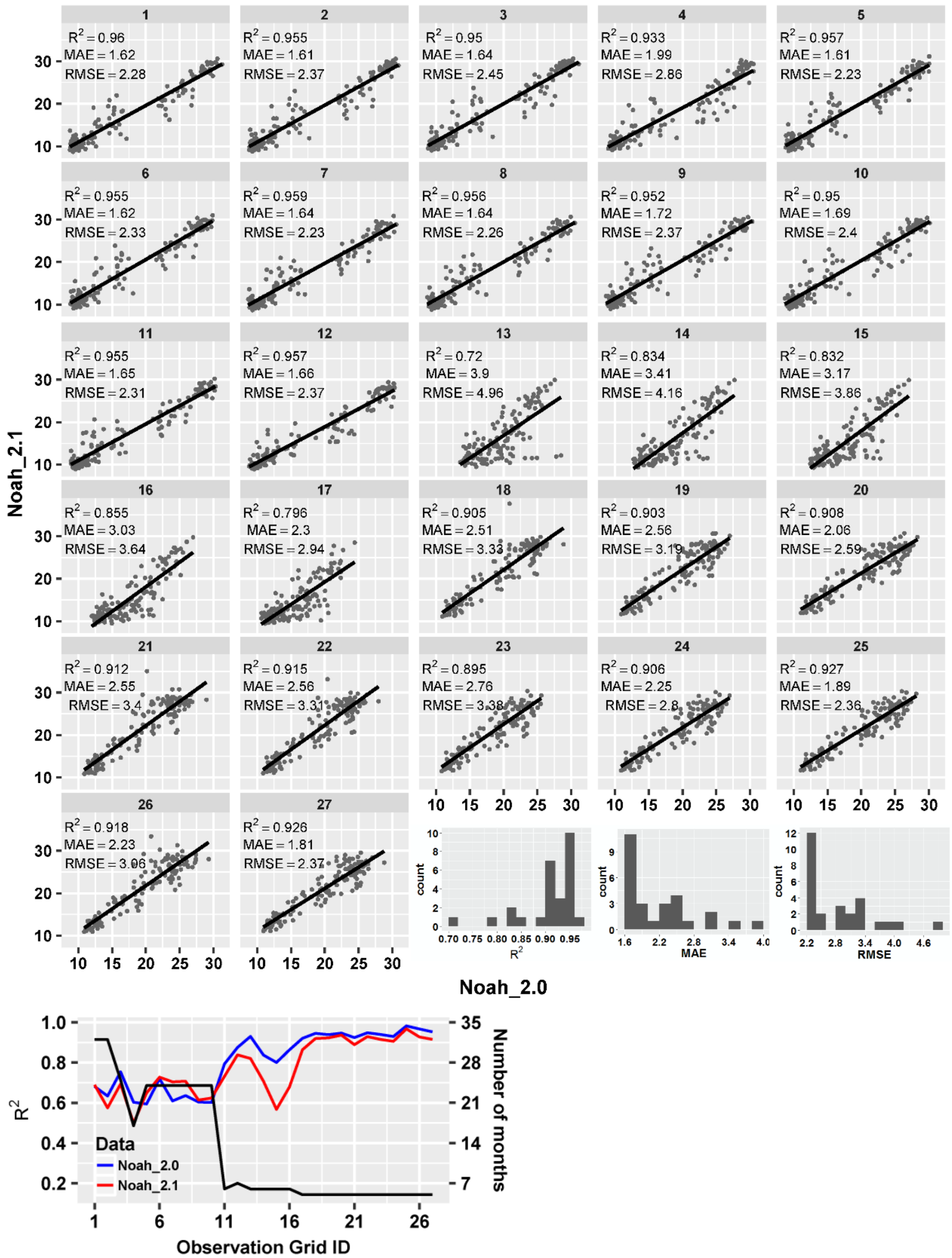

Fig. 3. Correlations between monthly Noah_2.0 soil moisture data and Noah_2.1 soil moisture data during 2008-2010 from the perspective of R^2, MAE (mean absolute error) and RMSE (root mean square error) for the period of 2000-2010 at 27 observation grids (the first panel). The histograms show the distribution of R^2, MAE and RMSE. In the bottom panel, the left axis shows changes of R^2 between Noah_2.0 soil moisture data (blue curve) and Noah_2.1 soil moisture data (red curve) with in-situ observed soil moisture data in different grids (Fig. 1); the right axis shows the number of months with time overlap, which is represented as a black line.

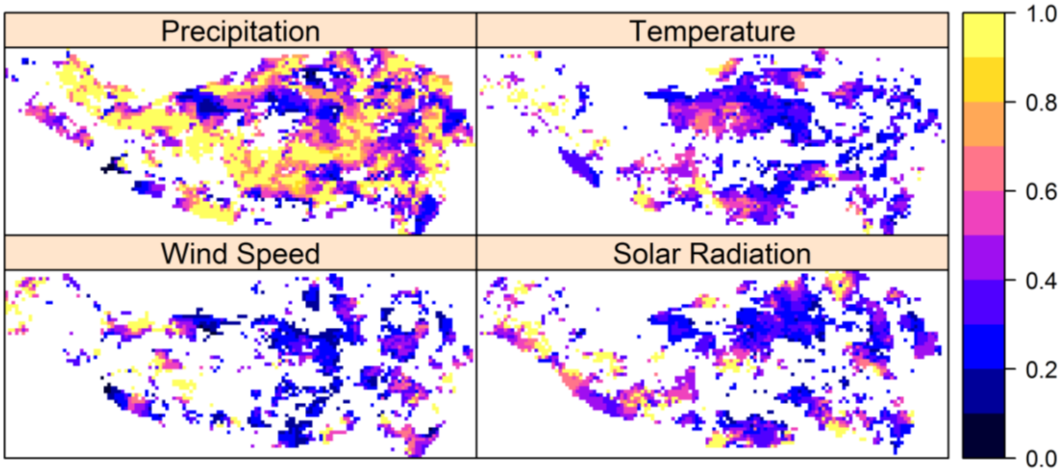

Fig. 4. Identification of major drivers for soil moisture changes (Noah_2.0) during 1979-2010 using stepwise regressive technique and multiple general linear model (GLM) regression. The stepwise regressive technique was used to screen out the principle drivers behind soil moisture changes, and the multiple general linear model (GLM) regression was used to quantify fractional contributions of each principle driver to soil moisture changes. The analysis was done on each pixel. The numbers marked by different colors denote the fractional contribution of each potential driver to soil moisture changes. Based on the spatial pattern of fractional contributions, precipitation acts as the major driver behind soil moisture changes across most regions of the HTP.

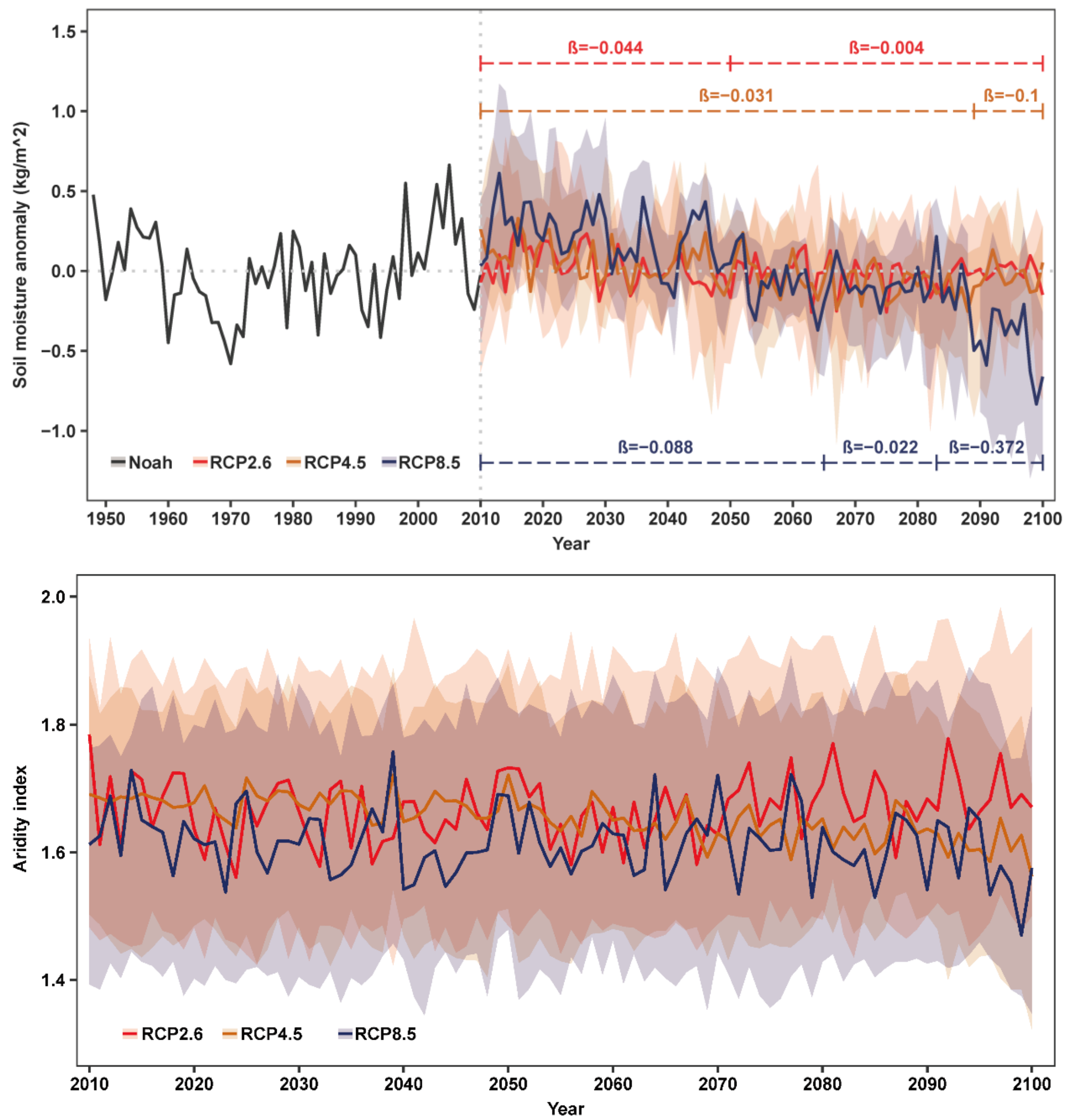

Fig. 5. Soil moisture anomaly during 1948-2010 and 2010-2100 based on remotely sensed and reanalysis soil moisture data in the whole Himalayan-Tibetan Plateau by 26 models under three scenarios: RCP2.6, RCP4.5 and RCP8.5. In the upper panel, the β values show changing rates of soil moisture during different time intervals (unit: $kg/m^2/10a$) by the Sen's slope method. The shaded areas denote the 95% confidence interval by Student-*t* distribution. The lower panel shows future changes of the aridity index based on remotely sensed and reanalysis dataset by 22 models under RCP2.6, RCP4.5 and RCP8.5 scenarios.

https://doi.org/10.1016/j.scitotenv.2018.12.209

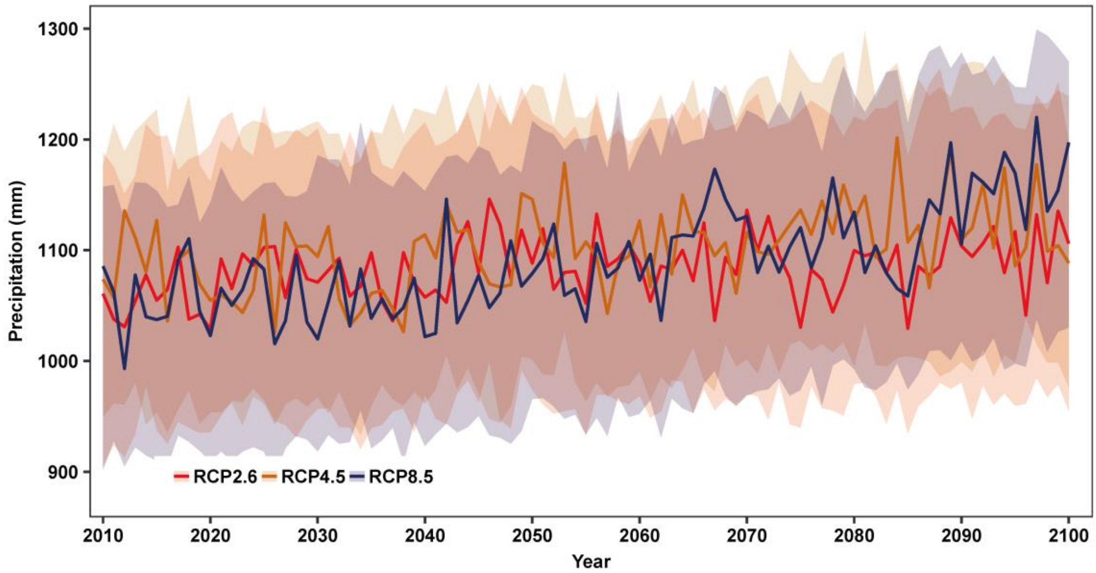

Fig. 6. Future changes of precipitation based on remotely sensed and reanalysis dataset by 40 models under RCP2.5, RCP4.6 and RCP8.5 scenarios (27 models for RCP2.6, 37 models for RCP4.5 and 40 models for RCP8.5).

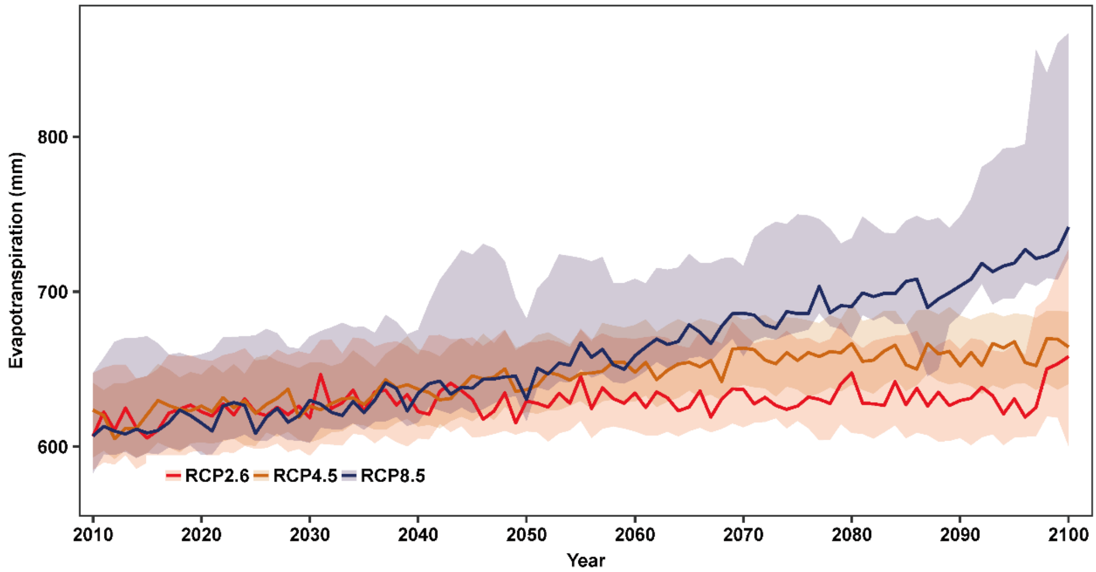

Fig. 7. Future changes of Penman-Monteith evapotranspiration based on remotely sensed and reanalysis dataset by 23 models under RCP2.6, RCP4.5 and RCP8.5 scenarios (15 models for RCP2.6, 23 models for RCP4.5 and 20 models for RCP8.5).

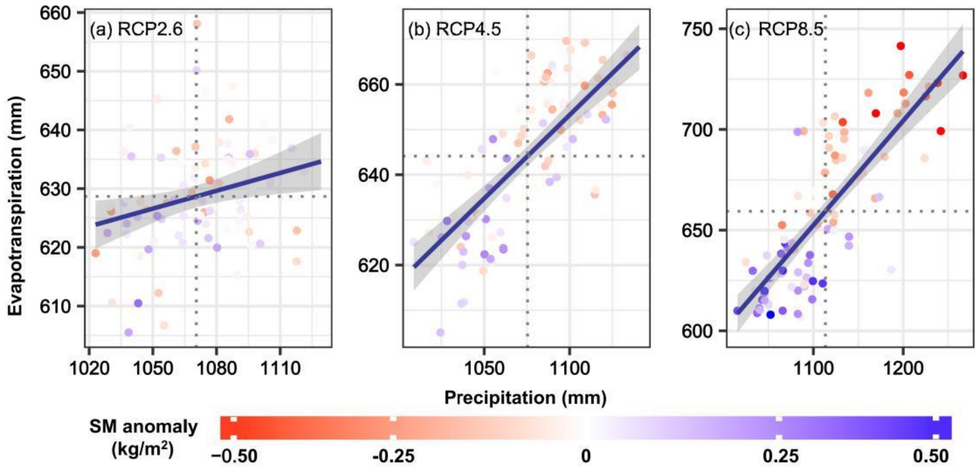

Fig. 8. Relationships between precipitation, evapotranspiration, and soil moisture anomaly in the future (2010-2100) under RCP2.6 (a), RCP4.5 (b) and RCP8.5 (c). Scatter points denote median values of precipitation, evapotranspiration, and soil moisture anomaly. The gray dashed lines indicate the mean values of precipitation (vertical) and evapotranspiration (horizontal). The blue lines shows fitted results by linear model with 95% confident interval.

https://doi.org/10.1016/j.scitotenv.2018.12.209

Table 1. 26 GCM models from CMIP5 with modelling results of the surface soil moisture under scenarios of RCP2.6, RCP4.5 and RCP8.5. The detailed information of model can be found in supplementary files.

Model Names				
ACCESS1.0	ACCESS1.3	CanESM2	CNRM-CM5	CSIRO-Mk3.6.0
FGOALS-g2	FGOALS-s2	GFDL-CM3	GFDL-ESM2G	GFDL-ESM2M
GISS-E2-H	GISS-E2-H-CC	GISS-E2-R	GISS-E2-R-CC	HadGEM2-CC
HadGEM2-ES	INM-CM4	IPSL-CM5A-LR	IPSL-CM5A-MR	IPSL-CM5B-LR
MIROC5	MIROC-ESM	MIROC-ESM-CHEM	MRI-CGCM3	NorESM1-M
NorESM1-ME				

Table 2. The statistical mean value for precipitation (Pr), evapotranspiration (ET), soil moisture anomaly (SMA) and aridity index (AI) in the future under three scenarios, that is, RCP2.6, RCP4.5 and RCP8.5. Slope is the coefficient of evapotranspiration with precipitation. P-value indicates whether or not there exists evident relationship.

Scenarios	Pr (mm)	ET (mm)	AI	SMA (10^{-3}kg/m^2)	Slope	P-value
RCP2.6	1070	629	1.66	0.5	0.10	0.102
RCP4.5	1075	644	1.65	-2.9	0.37	0
RCP8.5	1113	659	1.61	6.5	0.52	0

https://doi.org/10.1016/j.scitotenv.2018.12.209

Supporting Information for

Is Himalayan-Tibetan Plateau Drying? Historical observations and future trends

Qiang Zhang[1,2,3]*, Keke Fan[1,2,3], Vijay P. Singh[4], Changqing Song[1,2,3], Chong-Yu Xu[5], Peng Sun[6]

1. Key Laboratory of Environmental Change and Natural Disaster, Ministry of Education, Beijing Normal University, Beijing 100875, China;

2. Faculty of Geographical Science, Academy of Disaster Reduction and Emergency Management, Ministry of Education/Ministry of Civil Affairs, Beijing Normal University, Beijing 100875, China;

3. State Key Laboratory of Earth Surface Processes and Resources Ecology, Beijing Normal University, Beijing 100875, China;

4. Department of Biological and Agricultural Engineering and Zachry Department of Civil Engineering, Texas A&M University, College Station, Texas, USA;

5. Department of Geosciences, Oslo University, Blindern 0316, Oslo, Norway;

6. College of Territorial Resource and Tourism, Anhui Normal University, Anhui 241002, China;

https://doi.org/10.1016/j.scitotenv.2018.12.209

Contents of this file

Fig. S1
Tables S1 to S4

Additional Supporting Information (Files uploaded separately)

Fig. S1. Comparison between soil moisture from five different data sources: In-situ, ECV, ERA, MERRA and Noah by averaging the values in the grids where there exist measuring stations in three different soil moisture networks: Ngari, Naqu and Maqu. The time span for the comparison of soil moisture datasets is from May, 2008 to September, 2014. The gray-shaded areas indicate the confidence interval of the in-situ observed soil moisture data by ARIMA method.

Table S1. Information on 100 in-situ stations for observed soil moisture on the Himalayan-Tibetan Plateau (HTP). The StationID is the unique identification or name of the stations. Lat is the latitude and Lon the longitude which jointly determine the locations of stations. Elev means the elevation of the in-situ stations. Source indicates where the data are derived from, i.e. Tibet-Obsa and/or CTP_SMTMN (ISMN)b. Location shows where the in-situ stations are located on the HTP. GridNum is the number of grids the in-situ stations are included in (Figure 1). Latgrid and Longrid are the latitude and longitude of center-point of the grid that the in-situ stations are located in.

Table S2. Information of soil moisture data by remotely sensed and reanalysis soil moisture datasets. Note that SDSR is the abbreviation of the surface downward shortwave radiation.

Table S3. 26 GCM models from CMIP5 with modelling results of the surface soil moisture under scenarios of RCP2.6, RCP4.5 and RCP8.5. The models with asterisk (*) are those models with soil moisture data that are in positive correlation with historical soil moisture.

Table S4. Information on models with variables for modelling of aridity index, terrestrial potential evapotranspiration, and precipitation under scenarios of RCP2.6, RCP4.5 and RCP8.5.

Introduction

In this study, we use a mass of data from totally different sources, including, in-situ soil moisture, based remotely sensing and reanalysis soil moisture, climate variables from the China Meteorological Forcing Dataset, soil moisture from outputs of 26 CMIP5 GCMs and climate variables of 41 CMIP5 GCMs under three scenarios, i.e., RCP2.6, RCP4.5, RCP8.5. In order to more clearly show readers the detail of the data, here we list all the data used, although these datasets have been described in details in the main text.

https://doi.org/10.1016/j.scitotenv.2018.12.209

Supplementary Figure

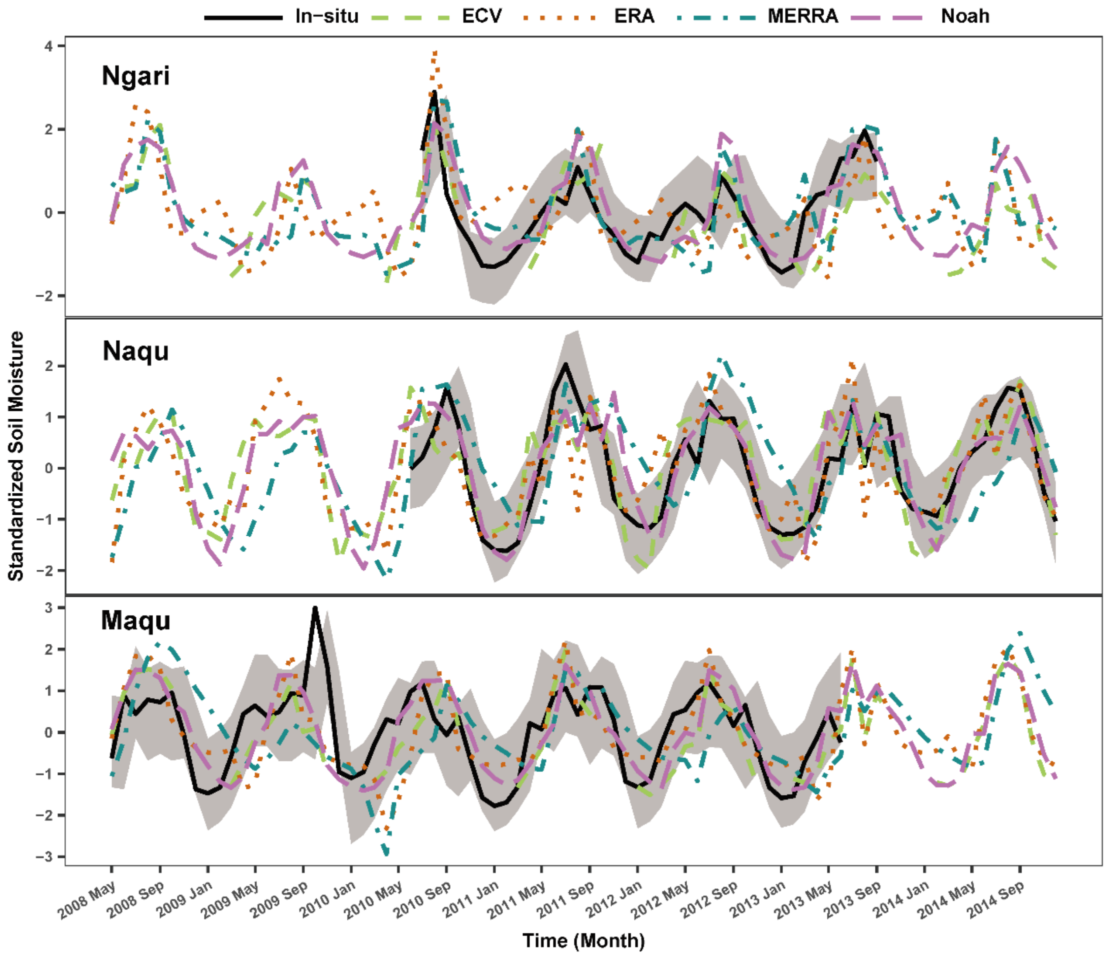

Fig. S1. Comparison between soil moisture from five different data sources: In-situ, ECV, ERA, MERRA and Noah by averaging the values in the grids where there exist measuring stations in three different soil moisture networks: Ngari, Naqu and Maqu. The time span for the comparison of soil moisture datasets is from May, 2008 to September, 2014. The gray-shaded areas indicate the confidence interval of the in-situ observed soil moisture data by ARIMA method.

https://doi.org/10.1016/j.scitotenv.2018.12.209

Supplementary Tables

Table S1. Information on 100 in-situ stations for observed soil moisture on the Himalayan-Tibetan Plateau (HTP). The StationID is the unique identification or name of the stations. Lat is the latitude and Lon the longitude which jointly determine the locations of stations. Elev means the elevation of the in-situ stations. Source indicates where the data are derived from, i.e. Tibet-Obs[a] and/or CTP_SMTMN (ISMN)[b]. Location shows where the in-situ stations are located on the HTP. GridNum is the number of grids the in-situ stations are included in (Figure 1). Latgrid and Longrid are the latitude and longitude of center-point of the grid that the in-situ stations are located in.

StationID	Lat	Lon	Elev	Source	Location	GridNum	Latgrid	Longrid
CST_01	33.88	102.13	3431	Tibet-Obs	Maqu	1	33.875	102.125
CST_02	33.67	102.13	3449	Tibet-Obs	Maqu	2	33.625	102.125
CST_03	33.90	101.97	3507	Tibet-Obs	Maqu	3	33.875	101.875
CST_04	33.77	101.72	3504	Tibet-Obs	Maqu	4	33.875	101.625
CST_05	33.67	101.88	3542	Tibet-Obs	Maqu	5	33.625	101.875
NST_01	33.88	102.13	3431	Tibet-Obs	Maqu	1	33.875	102.125
NST_02	33.88	102.13	3434	Tibet-Obs	Maqu	1	33.875	102.125
NST_03	33.77	102.13	3513	Tibet-Obs	Maqu	1	33.875	102.125
NST_04	33.62	102.05	3448	Tibet-Obs	Maqu	2	33.625	102.125
NST_05	33.63	102.05	3476	Tibet-Obs	Maqu	2	33.625	102.125
NST_06	34.00	102.27	3428	Tibet-Obs	Maqu	6	34.125	102.375
NST_07	33.98	102.35	3430	Tibet-Obs	Maqu	7	33.875	102.375
NST_08	33.97	102.60	3473	Tibet-Obs	Maqu	8	33.875	102.625
NST_09	33.90	102.55	3434	Tibet-Obs	Maqu	8	33.875	102.625
NST_10	33.85	102.57	3512	Tibet-Obs	Maqu	8	33.875	102.625
NST_11	33.68	102.47	3442	Tibet-Obs	Maqu	9	33.625	102.375
NST_12	33.62	102.47	3441	Tibet-Obs	Maqu	9	33.625	102.375
NST_13	34.02	101.93	3519	Tibet-Obs	Maqu	10	34.125	101.875
NST_14	33.92	102.12	3432	Tibet-Obs	Maqu	1	33.875	102.125
NST_15	33.85	101.88	3752	Tibet-Obs	Maqu	3	33.875	101.875
Ali01	33.43	79.73	4262	Tibet-Obs	Ngari	11	33.375	79.625
Ali02	33.45	79.62	4266	Tibet-Obs	Ngari	11	33.375	79.625
Ali03	33.45	79.62	4261	Tibet-Obs	Ngari	11	33.375	79.625
Naqu_BJ	31.37	91.88	4509	Tibet-Obs	Naqu	12	31.375	91.875
Naqu_East	31.37	91.92	4527	Tibet-Obs	Naqu	12	31.375	91.875
Naqu_North	31.37	91.87	4507	Tibet-Obs	Naqu	12	31.375	91.875
Naqu_South	31.32	91.87	4510	Tibet-Obs	Naqu	12	31.375	91.875
Naqu_West	31.33	91.82	4506	Tibet-Obs	Naqu	12	31.375	91.875

Sq01	32.48	80.07	4306	Tibet-Obs	Ngari	13	32.375	80.125
Sq02	32.50	80.02	4304	Tibet-Obs	Ngari	14	32.625	80.125
Sq03	32.50	79.97	4278	Tibet-Obs	Ngari	15	32.625	79.875
Sq04	32.50	79.97	4269	Tibet-Obs	Ngari	15	32.625	79.875
Sq05	32.50	79.92	4261	Tibet-Obs	Ngari	15	32.625	79.875
Sq06	32.50	79.87	4257	Tibet-Obs	Ngari	15	32.625	79.875
Sq07	32.52	79.83	4280	Tibet-Obs	Ngari	15	32.625	79.875
Sq08	32.55	79.83	4306	Tibet-Obs	Ngari	15	32.625	79.875
Sq09	32.45	80.05	4275	Tibet-Obs	Ngari	13	32.375	80.125
Sq10	32.42	80.00	4275	Tibet-Obs	Ngari	13	32.375	80.125
Sq11	32.45	79.97	4274	Tibet-Obs	Ngari	16	32.375	79.875
Sq12	32.45	79.93	4264	Tibet-Obs	Ngari	16	32.375	79.875
Sq13	32.43	79.90	4292	Tibet-Obs	Ngari	16	32.375	79.875
Sq14	32.45	80.17	4368	Tibet-Obs	Ngari	13	32.375	80.125
Sq16	32.43	80.07	4288	Tibet-Obs	Ngari	13	32.375	80.125
BC02	31.07	92.37	4835	ISMN	Naqu	17	31.125	92.375
BC03	31.11	92.31	4690	ISMN	Naqu	17	31.125	92.375
BC04	31.13	92.25	4609	ISMN	Naqu	17	31.125	92.375
BC05	31.17	92.20	4548	ISMN	Naqu	18	31.125	92.125
BC06	31.23	92.16	4491	ISMN	Naqu	18	31.125	92.125
BC07	31.27	92.11	4478	ISMN	Naqu	19	31.375	92.125
BC08	31.33	92.04	4470	ISMN	Naqu	19	31.375	92.125
CD01	31.71	92.46	4762	ISMN	Naqu	20	31.625	92.375
CD02	31.68	92.41	4612	ISMN	Naqu	20	31.625	92.375
CD03	31.66	92.34	4518	ISMN	Naqu	20	31.625	92.375
CD04	31.64	92.33	4491	ISMN	Naqu	20	31.625	92.375
CD05	31.59	92.24	4637	ISMN	Naqu	21	31.625	92.125
CD06	31.54	92.21	4769	ISMN	Naqu	21	31.625	92.125
CD07	31.50	92.13	4628	ISMN	Naqu	19	31.375	92.125
MS3475	31.95	91.72	4637	ISMN	Naqu	22	31.875	91.625
MS3482	31.89	91.70	4713	ISMN	Naqu	22	31.875	91.625
MS3488	31.84	91.71	4799	ISMN	Naqu	22	31.875	91.625
MS3494	31.81	91.75	4818	ISMN	Naqu	22	31.875	91.625
MS3501	31.75	91.78	4723	ISMN	Naqu	23	31.875	91.875
MS3506	31.72	91.81	4684	ISMN	Naqu	24	31.625	91.875
MS3513	31.68	91.84	4628	ISMN	Naqu	24	31.625	91.875
MS3518	31.66	91.79	4574	ISMN	Naqu	24	31.625	91.875
MS3523	31.64	91.75	4570	ISMN	Naqu	24	31.625	91.875
MS3527	31.61	91.74	4552	ISMN	Naqu	25	31.625	91.625
MS3533	31.59	91.79	4539	ISMN	Naqu	24	31.625	91.875

MS3538	31.58	91.84	4575	ISMN	Naqu	24	31.625	91.875
MS3545	31.57	91.91	4671	ISMN	Naqu	24	31.625	91.875
MS3552	31.55	91.98	4574	ISMN	Naqu	24	31.625	91.875
MS3559	31.53	92.05	4516	ISMN	Naqu	21	31.625	92.125
MS3576	31.41	91.97	4517	ISMN	Naqu	12	31.375	91.875
MS3593	31.30	91.85	4574	ISMN	Naqu	12	31.375	91.875
MS3603	31.26	91.80	4630	ISMN	Naqu	12	31.375	91.875
MS3614	31.17	91.76	4633	ISMN	Naqu	26	31.125	91.875
MS3620	31.13	91.73	4765	ISMN	Naqu	27	31.125	91.625
MS3627	31.09	91.69	4736	ISMN	Naqu	27	31.125	91.625
MS3633	31.03	91.68	4675	ISMN	Naqu	27	31.125	91.625
MSNQRW	31.46	92.02	4537	ISMN	Naqu	19	31.375	92.125
MSBJ	31.37	91.90	4505	ISMN	Naqu	12	31.375	91.875
P1	31.78	91.73	4730	ISMN	Naqu	22	31.875	91.625
P2	31.74	91.73	4677	ISMN	Naqu	25	31.625	91.625
P3	31.69	91.72	4600	ISMN	Naqu	25	31.625	91.625
P5	31.61	91.91	4780	ISMN	Naqu	24	31.625	91.875
P7	31.67	91.90	4737	ISMN	Naqu	24	31.625	91.875
P8	31.74	91.87	4665	ISMN	Naqu	24	31.625	91.875
P9	31.73	91.77	4758	ISMN	Naqu	24	31.625	91.875
P10	31.81	91.85	4804	ISMN	Naqu	23	31.875	91.875
P11	31.82	91.80	4953	ISMN	Naqu	23	31.875	91.875
C1	31.68	91.77	4647	ISMN	Naqu	24	31.625	91.875
C2	31.69	91.81	4672	ISMN	Naqu	24	31.625	91.875
C3	31.61	91.77	4585	ISMN	Naqu	24	31.625	91.875
C4	31.62	91.84	4608	ISMN	Naqu	24	31.625	91.875
F1	31.69	91.80	4699	ISMN	Naqu	24	31.625	91.875
F2	31.70	91.79	4697	ISMN	Naqu	24	31.625	91.875
F3	31.72	91.80	4699	ISMN	Naqu	24	31.625	91.875
F4	31.70	91.77	4737	ISMN	Naqu	24	31.625	91.875
F5	31.69	91.79	4719	ISMN	Naqu	24	31.625	91.875
BC	31.37	91.98	4559	ISMN	Naqu	12	31.375	91.875

Note: a: Third Pole Environment Database: http://www.tpedatabase.cn/portal/ index.jsp; b: Central Tibetan Plateau Soil Moisture and Temperature Monitoring Network (version 2) in the International Soil Moisture Network (ISMN): http://ismn.geo.tuwien.ac.at/.

https://doi.org/10.1016/j.scitotenv.2018.12.209

Table S2. Information of soil moisture data by remotely sensed and reanalysis soil moisture datasets. Note that SDSR is the abbreviation of the surface downward shortwave radiation.

Datasets	Duration	Spatial scale	Spatial resolution (lon×lat)
ECV	1979-2014	global	0.25×0.25
ERA-Interm	1979-2016	global	0.25×0.25
MERRA	1980-present	global	0.625×0.5
Noah_2.0(GLDAS)	1948-2010	quasi-global	0.25×0.25
Noah_2.1(GLDAS)	2000-present	quasi-global	0.25×0.25
Precipitation	1979-2010	China	0.1×0.1
Temperature	1979-2010	China	0.1×0.1
Wind velocity	1979-2010	China	0.1×0.1
SDSR	1979-2010	China	0.1×0.1

https://doi.org/10.1016/j.scitotenv.2018.12.209

Table S3. 26 GCM models from CMIP5 with modelling results of the surface soil moisture under scenarios of RCP2.6, RCP4.5 and RCP8.5. The models with asterisk (*) are those models with soil moisture data that are in positive correlation with historical soil moisture.

No.	Model name	Institute ID	Resolution (Lon×lat)	Historical	RCP2.6	RCP4.5	RCP8.5
1	ACCESS1.0	CSIRO-BOM	192×145	185001-200512		200601-210012	200601-210012
2*	ACCESS1.3	CSIRO-BOM	192×145	185001-200512		200601-210012	200601-210012
3	CanESM2	CCCMA	128×64	185001-200512	200601-230012	200601-230012	200601-210012
4*	CNRM-CM5	CNRM-CERFACS	256×128	185001-200512	200601-210012	200601-230012	200601-230012
5*	CSIRO-Mk3.6.0	CSIRO-QCCCE	192×96	185001-200512	200601-210012	200601-230012	200601-230012
6*	FGOALS-g2	LASG-GESS	128×60	185001-200612	200601-210112		200601-210112
7	FGOALS-s2	LASG-IAP	128×108	185001-200512	200601-210012		200601-210012
8	GFDL-CM3	NOAA-GFDL	144×90	186001-200512	200601-210012	200601-210012	200601-210012
9	GFDL-ESM2G	NOAA-GFDL	144×90	186101-200512	200601-210012	200601-210012	200601-210012
10	GFDL-ESM2M	NOAA-GFDL	144×90	186101-200512	200601-210012	200601-210012	200601-210012
11*	GISS-E2-H	NASA-GISS	144×90	185001-200512	200601-230012	200601-230012	200601-230012
12	GISS-E2-H-CC	NASA-GISS	144×90	185001-201012		200601-210012	200601-210012
13	GISS-E2-R	NASA-GISS	144×90	185001-200512	200601-230012	200601-230012	200601-230012
14	GISS-E2-R-CC	NASA-GISS	144×90	185001-201012		200601-210012	200601-210012
15	HadGEM2-CC	MOHC	192×145	185912-200511		200512-210012	200512-210012
16	HadGEM2-ES	MOHC	192×145	185912-200511	200512-229912	200512-229912	200512-229912
17	INM-CM4	INM	180×120	185001-200512		200601-210012	200601-210012
18	IPSL-CM5A-LR	IPSL	96×96	185001-200512	200601-230012	200601-230012	200601-230012
19*	IPSL-CM5A-MR	IPSL	144×143	185001-200512	200601-210012	200601-230012	200601-210012
20*	IPSL-CM5B-LR	IPSL	96×96	185001-200512		200601-210012	200601-210012
21*	MIROC5	MIROC	256×128	185001-201212	200601-230012	200601-210012	200601-210012
22*	MIROC-ESM	MIROC	128×64	185001-200512	200601-210012	200601-230012	200601-210012
23*	MIROC-ESM-CHEM	MIROC	128×64	185001-200512	200601-210012	200601-210012	200601-210012
24	MRI-CGCM3	MRI	320×260	185001-200512	200601-210012	200601-210012	200601-210012
25	NorESM1-M	NCC	144×96	185001-200512	200601-210012	200601-230012	200601-210012

26*	NorESM1-ME	NCC	144×96	185001-200512	200601-210112	200601-210212	200601-210012

Note: All CMIP5 data are derived from https://esgf-node.llnl.gov/projects/esgf-llnl/.

Table S4. Information on models with variables for modelling of aridity index, terrestrial potential evapotranspiration, and precipitation under scenarios of RCP2.6, RCP4.5 and RCP8.5.

		Precipitation (pr)			Max Temperature (tasmax)			Min Temperature (tasmin)			Relative humidity (hurs)			Wind speed (sfcWind)		
	Model name	RCP2.6	RCP4.5	RCP8.5	RCP2.6	RCP4.5	RCP8.5	RCP2.6	RCP4.5	RCP8.5	RCP2.6	RCP4.5	RCP8.5	RCP2.6	RCP4.5	RCP8.5
1	ACCESS1-0	√	√			√	√		√	√		√	√		√	√
2	ACCESS1-3	√	√			√	√		√	√		√	√		√	√
3	bcc-csm1-1-m	√	√	√												
4	bcc-csm1-1	√	√	√												
5	BNU-ESM	√	√	√												
6	CanESM2	√	√	√	√	√	√	√	√	√	√	√	√	√	√	√
7	CCSM4	√	√	√												
8	CESM1-BGC	√	√													
9	CESM1-CAM5	√	√	√												
10	CMCC-CESM	√														
11	CMCC-CM	√	√													
12	CMCC-CMS	√	√													
13	CNRM-CM5	√	√	√	√	√	√	√	√	√	√	√	√	√	√	√
14	CSIRO-Mk3-6-0	√	√	√												
15	EC-EARTH	√														
16	FGOALS-g2	√	√	√												
17	FIO-ESM	√	√	√												
18	GEOSCCM					√			√			√			√	
19	GFDL-CM3	√	√	√	√	√	√	√	√	√	√	√	√	√	√	√
20	GFDL-ESM2G	√	√	√	√	√	√	√	√	√	√	√	√	√	√	√
21	GFDL-ESM2M	√	√	√	√	√	√	√	√	√	√	√	√	√	√	√
22	GISS-E2-H	√	√	√	√	√	√	√	√	√	√	√	√	√	√	√
23	GISS-E2-R	√	√	√	√	√	√	√	√	√	√	√	√	√	√	√
24	GISS-E2-H-CC	√	√			√			√			√			√	
25	GISS-E2-R-CC	√	√			√			√			√			√	
26	HadGEM2-AO	√	√	√	√	√	√	√	√	√	√	√	√	√	√	√
27	HadGEM2-CC	√	√			√	√		√	√		√	√		√	√
28	HadGEM2-ES	√	√	√	√	√	√	√	√	√	√	√	√	√	√	√
29	inmcm4	√	√			√	√		√	√		√	√		√	√
30	IPSL-CM5A-LR	√	√	√	√	√	√	√	√	√	√	√	√	√	√	√
31	IPSL-CM5A-MR	√	√	√	√	√	√	√	√	√	√	√	√	√	√	√
32	IPSL-CM5B-LR	√	√			√	√		√	√		√	√		√	√

https://doi.org/10.1016/j.scitotenv.2018.12.209

33	MIROC-ESM-CHEM	√	√	√	√	√	√	√	√	√	√	√	√	√	√	√
34	MIROC-ESM	√	√	√	√	√	√	√	√	√	√	√	√	√	√	√
35	MIROC5	√	√	√	√	√	√	√	√	√	√	√	√	√	√	√
36	MPI-ESM-LR	√	√	√												
37	MPI-ESM-MR	√	√	√												
38	MRI-ESM1	√														
39	MRI-CGCM3	√	√	√	√	√	√	√	√	√	√	√	√	√	√	√
40	NorESM1-M	√	√	√												
41	NorESM1-ME	√	√	√												